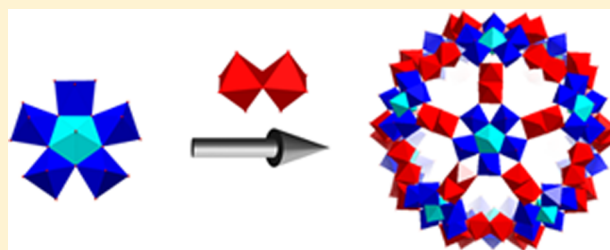


Direct Observation of the Formation Pathway of  $[\text{Mo}_{132}]$  KepleratesSubharanjan Biswas,<sup>†</sup> Dolores Melgar,<sup>‡,§</sup> Amitava Srimany,<sup>||</sup> Antonio Rodríguez-Fortea,<sup>⊥</sup> Thalappil Pradeep,<sup>\*,||</sup> Carles Bo,<sup>\*,‡</sup> Josep M. Poblet,<sup>\*,⊥</sup> and Soumyajit Roy<sup>\*,†</sup><sup>†</sup>Eco-Friendly Applied Materials Laboratory (EFAML), Materials Science Centre, Department of Chemical Sciences, Indian Institute of Science Education and Research-Kolkata (IISER-Kolkata), Mohanpur Campus, Mohanpur 741246, India<sup>‡</sup>Institute of Chemical Research of Catalonia (ICIQ), Av. Països Catalans 16, 43007 Tarragona, Spain<sup>§</sup>Departament d'Enginyeria Química, ETSEQ, Universitat Rovira i Virgili, Av. dels Països Catalans, 26, 43007 Tarragona, Spain<sup>||</sup>Department of Chemistry, Indian Institute of Technology Madras, Chennai 600036, India<sup>⊥</sup>Departament de Química Física i Inorgànica, Universitat Rovira i Virgili, Marcel·lí Domingo 1, 43007 Tarragona, Spain

## S Supporting Information

**ABSTRACT:** The formation pathway of a closed spherical cluster  $[\text{Mo}_{132}]$ , starting from a library of building blocks of molybdate anions, has been reported. Electrospray ionization mass spectrometry, Raman spectroscopy, and theoretical studies describe the formation of such a complex cluster from a reduced and acidified aqueous solution of molybdate. Understanding the emergence of such an enormous spherical model cluster may lead to the design of new clusters in the future. Formation of such a highly symmetric cluster is principally controlled by charge balance and the emergence of more symmetric structures at the expense of less symmetric ones.



## ■ INTRODUCTION

Polyoxometalate (POM)<sup>1,2</sup> clusters are polyatomic ions, usually anions, that consist of transition metals like Mo, V, and W linked together by shared oxygen atoms to form closed three-dimensional (3D) frameworks. Because of the various sizes, structures, and elemental compositions, a wide range of properties and a correspondingly wide range of potential applications are observed in POMs, for instance, in catalysis,<sup>3</sup> in energy production and storage,<sup>4</sup> and in medicinal chemistry.<sup>5</sup>  $[\text{Mo}_{132}]$ <sup>6,7</sup> Keplerate,<sup>8</sup> first reported by Müller et al.,<sup>9</sup> is synthesized by partial reduction of Mo(VI) atoms present in  $(\text{NH}_4)_6\text{Mo}_7\text{O}_{24}$ .  $[\text{Mo}_{132}]$  is a type of molybdenum brown Keplerate anion with a diameter of 2.9 nm. The structure of  $[\text{Mo}_{132}]$  was determined by single-crystal X-ray diffraction (SC-XRD) studies by the Bielefeld group of A. Müller.<sup>7</sup> This spherical cluster contains 132 molybdenum centers; 72 molybdenum centers are in the +VI oxidation state, and the rest of the 60 molybdenum centers are in the +V oxidation state. The dark brown color of  $[\text{Mo}_{132}]$  arises from intervalence charge transfer between the  $\text{Mo}^{\text{V}}$  and  $\text{Mo}^{\text{VI}}$  centers. Moreover, such POMs superassemble to form blackberry type soft oxometalate (SOM)<sup>10–12</sup> superstructures of larger dimensions.<sup>13,14</sup> Herein, we investigate and present direct experimental evidence [electrospray ionization mass spectrometry (ESI-MS) and Raman spectroscopic studies] along with computational studies to show the pathway of formation of such clusters under prevalent chemical conditions.

A  $[\text{Mo}_{132}]$  type Keplerate cluster assembled with acetate as the ligand has icosahedral point group symmetry.<sup>15</sup> The cluster structure from a building block approach is envisaged as follows. Twelve pentagonal  $[(\text{Mo})\text{Mo}_5]$  building blocks are disposed at the vertices of an icosahedron.<sup>16,17</sup>  $[(\text{Mo})\text{Mo}_5]$  building blocks are formed with central pentagonal bipyramidal  $[\text{MoO}_7]$  linked to five  $[\text{MoO}_6]$  octahedra through edges, which shows an overall icosahedral symmetry (Figure 1). Disposition of 12  $[(\text{Mo})\text{Mo}_5]$  blocks at the vertices of the icosahedron creates space for 30 linkers on the icosahedron's surface to be accommodated (following Euler's theorem)<sup>18</sup> and linked simultaneously to the prevalent pentagonal building blocks.

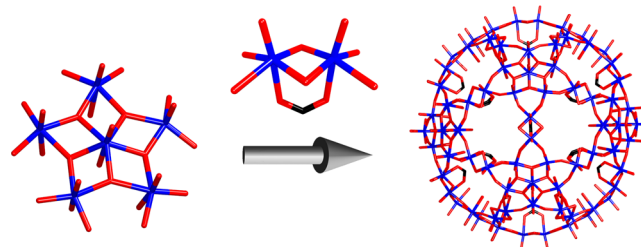


**Figure 1.** Formation of the 3D structure of the  $[\text{Mo}_{132}]$  cluster from  $[(\text{Mo})\text{Mo}_5]$  and  $[\text{Mo}_2(\text{CH}_3\text{COO})]$  building blocks shown in a wireframe model. Blue color represents Mo, red O, and black acetate.

Received: November 6, 2015

Published: August 25, 2016

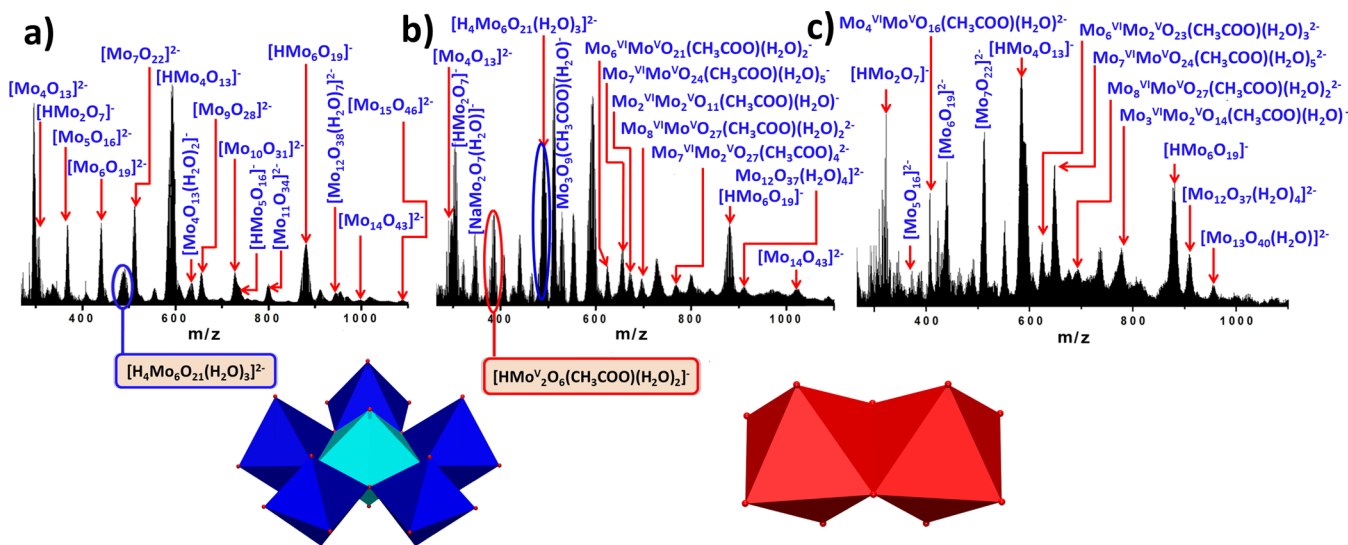


**Figure 2.** ESI mass spectra during different steps of  $[\text{Mo}_{132}]$  formation. (a) Spectra of a colorless water solution of ammonium heptamolybdate, where the presence of  $[(\text{Mo})\text{Mo}_5]$  is evidenced as  $[\text{H}_4\text{Mo}_6\text{O}_{21}(\text{H}_2\text{O})_3]^{2-}$ . (b) Spectra of a solution after complete reduction by  $\text{N}_2\text{H}_4\text{SO}_4$ , which turns the solution green, where  $[\text{Mo}_2]$  is evidenced as  $[\text{HMo}_2\text{O}_6(\text{CH}_3\text{COO})(\text{H}_2\text{O})_2]^-$ . (c) Mass spectrum 12 h after the addition of all the reagents.

In the case of  $[\text{Mo}_{132}]$  with acetate as the ligand to the linkers, the linkers are  $[\text{Mo}_2(\text{CH}_3\text{COO})]$ . (Note that we omit the oxygen atoms from the formula of the cluster for the sake of simplicity.) Hence, the overall cluster formulation is determined to be  $[\text{pentagon}]_{12}[\text{linker}]_{30}$ ,  $[(\text{Mo})\text{Mo}_5]_{12}[\text{Mo}_2(\text{acetate})]_{30}$ ,  $[\text{Mo}_{132}(\text{acetate})_{30}]$ ,  $[\text{Mo}_{132}]$ , or **1** (Figure 1)  $(\text{NH}_4)_{42}\{[(\text{Mo}^{\text{VI}})\text{Mo}_5\text{O}_{21}(\text{H}_2\text{O})_6]_{12}\{[\text{Mo}^{\text{V}}\text{O}_4(\text{CH}_3\text{COO})]_{30}\} \approx [10\text{CH}_3\text{COONH}_4 \sim 300\text{H}_2\text{O}] \equiv (\text{NH}_4)_{42} \mathbf{1a} \equiv \mathbf{1}$ .

These clusters have been popularly called Keplerates because of their structural similarity to Kepler's early model of the universe.<sup>19</sup> Rather recently, inorganic cell-like behavior and receptive behavior have been found to be characteristics of these Keplerates.<sup>20–29</sup>

Such attributes characterize the Keplerates as an attractive model system for investigating the emergence of complexity<sup>30</sup> and symmetry in chemistry. In understanding such emergence, the first question would be how does such a complex icosahedral cluster<sup>31</sup> like  $[\text{Mo}_{132}]$  emerge from constituents of molybdates, reducing agents, and a buffer.

Before we proceed further, it is important to look at the general synthetic conditions of the cluster as reported in the literature, which we investigated in detail. The synthesis of the cluster involves the following key steps: (1) dissolution of molybdate in water, (2) reduction of the reaction mixture, and (3) acidification of the resulting solution.<sup>32</sup> The cluster so synthesized is highly charged. Hence, it is logical to think that understanding the formation of this cluster would require a technique that can observe such charged objects and its constituents. We chose ESI-MS to monitor such a formation pathway, along with Raman spectroscopy and theoretical calculations. Needless to say, ESI-MS<sup>33–35</sup> and theoretical calculations<sup>36–38</sup> have been extensively used to understand the formation of smaller polyoxometalate clusters. Raman spectroscopy has also been used in this study to investigate the solution stability of the related Keplerates. Müller et al. have previously reported the self-assembly of  $[\text{Mo}_{132}]$  with the help of Raman spectroscopy.<sup>39</sup> They have shown that addition of dinuclear  $[\text{Mo}_2]$  units to a dynamic library containing molybdates results in the spontaneous self-assembly of

$[\text{Mo}_{132}]$ , while the required pentagonal  $[(\text{Mo})\text{Mo}_5]$  building blocks are immediately formed. The reason to use Raman spectroscopy is the easy detection of the integrity of the  $[\text{Mo}_{132}]$  cluster from the Raman fingerprint. The quasi-spherical (icosahedral) construction of this cluster not only enhances its stability but also provides an easy Raman spectroscopic fingerprint for studying its stability. Because of the high  $I_h$  symmetry of such a cluster, only a few well-defined Raman lines are observed (note the presence of a 5-fold degeneracy, and that only  $A_g$  and  $H_g$  symmetric vibrational modes are Raman-allowed).<sup>40</sup> The Raman spectrum of a  $[\text{Mo}_{132}]$  type cluster shows four bands:  $950\text{ cm}^{-1}$  [ $\nu(\text{Mo}=\text{O}_i)$ ],  $880\text{ cm}^{-1}$  [ $\nu(\text{O}_{\text{br}}\text{breathing})$ ],  $374\text{ cm}^{-1}$  [ $\delta(\text{Mo}=\text{O}_i)$ ], and  $314\text{ cm}^{-1}$  [ $\delta(\text{Mo}-\text{O}-\text{Mo})$ ].<sup>41</sup> We monitored the reaction in all detailed steps of its formation; however, it was only the aforementioned three key steps during which significant changes were found to occur. In this paper, we will describe those changes to explain the formation of the  $[\text{Mo}_{132}]$  cluster.

## EXPERIMENTAL SECTION

**ESI-MS Experiment and Analyses.** ESI-MS was performed in a LTQ XL mass spectrometer from Thermo Scientific that has an ion trap mass analyzer. The sample was introduced into the system by direct infusion from a syringe at a constant flow rate of  $10\ \mu\text{L}/\text{min}$ . All the spectra were recorded in negative ion mode keeping the spray voltage at 5 kV, the sheath gas flow rate at 8 (manufacturer's unit), the capillary voltage at  $-35\text{ V}$ , the capillary temperature at  $150\text{ }^\circ\text{C}$ , and the tube lens voltage at  $-110\text{ V}$ . In each case, the spectrum shown is an average of 500 scans.

Mass spectra were recorded during each step of  $\text{Mo}_{132}$  synthesis. The first is the aqueous solution of ammonium heptamolybdate, followed by the addition of  $\text{CH}_3\text{COONH}_4$ . Next, the spectrum was recorded with the completely reduced green solution after the addition of  $\text{N}_2\text{H}_4\text{SO}_4$ . Then the solution was acidified via the addition of  $\text{CH}_3\text{COOH}$ , and the spectrum was recorded. To gain insight into the self-assembly process, spectra were recorded at different times after  $\text{CH}_3\text{COOH}$  addition, viz., after 30 min, 60 min, 2 h, 3 h, 24 h, 36 h, and 72 h. For all the mass spectral experiments, an aliquot of  $10\ \mu\text{L}$  was diluted with 1 mL of a 1:1 (v/v) mixture of acetonitrile and water. From the mixture,  $100\ \mu\text{L}$  was further diluted with 1 mL of a 1:1 (v/v) mixture of acetonitrile and water.

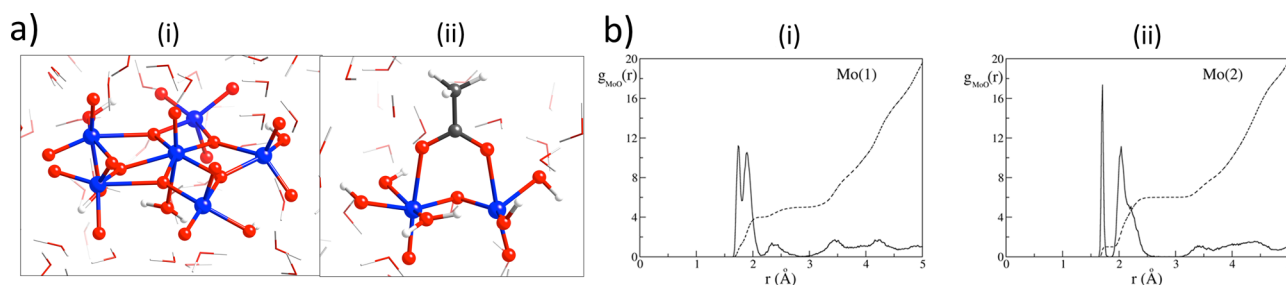


**Figure 3.** (a) Snapshots of the Carr–Parrinello molecular dynamics trajectories of protonated starlike hexamolybdate  $[\text{Mo}_6\text{O}_{18}(\text{OH})_3]^{3-}$  (i) and  $[\text{Mo}_2\text{V}_2\text{O}_3(\text{OH})_4(\text{H}_2\text{O})\text{CH}_3\text{COO}]^-$  dimer (ii). (b) Mo–O radial distribution functions (—) and their integrations, the coordination number (⋯), of the two  $\text{Mo}^{\text{V}}$  ions, Mo(1) and Mo(2), for 27 ps of simulation starting from  $[\text{Mo}_2\text{V}_2\text{O}_2(\text{OH})_6(\text{CH}_3\text{COO})]^-$ .

**Raman Spectroscopy.** Raman spectroscopy measurements were taken in the range of 200–1500  $\text{cm}^{-1}$  using the micro-Raman spectrometer LABRAM HR from Horiba Jobin Yvon with a grating of 1800 grooves/mm. All the experiments were performed using an excitation wavelength of 633 nm of an Ar ion laser, and the spectral resolution was 2  $\text{cm}^{-1}$ . The Raman spectrometer was calibrated prior to measurements using a Si wafer by the wavenumber shift calibration method. Solution phase Raman spectroscopy of the reaction system has been performed in a manner similar to that of ESI-MS experiments. Raman spectra have been recorded during different steps of the formation of the  $\text{Mo}_{132}$  cluster.

**Theoretical Calculations.** A detailed description of the Carr–Parrinello molecular dynamics simulations and density functional theory (DFT)-based Raman spectral calculations are included in the Supporting Information.

## RESULTS AND DISCUSSION

**ESI-MS Analysis of the Dissolution and Reduction Steps in the Formation of  $\text{Mo}_{132}$ .** The first ESI mass spectrum recorded after the addition of ammonium heptamolybdate in water is dominated by peaks of isopolymolybdate fragments of the  $[\text{Mo}_7\text{O}_{24}]^{6-}$  anion. In the negative ion mode investigation of the mass spectrum of  $(\text{NH}_4)_6\text{Mo}_7\text{O}_{24}$  and an ammonium acetate solution, predominantly members of two ion series are observed, namely,  $[\text{HMo}_m\text{O}_{3m+1}]^-$  ions such as  $[\text{HMo}_3\text{O}_{10}]^-$ ,  $[\text{HMo}_4\text{O}_{13}]^-$  etc., and  $[\text{Mo}_m\text{O}_{3m+1}]^{2-}$  ions such as  $[\text{Mo}_6\text{O}_{19}]^{2-}$ ,  $[\text{Mo}_9\text{O}_{28}]^{2-}$  (Figure 2a).<sup>42,43</sup> The dominance of the isopolymolybdates shows that the simple dissolution of the  $[\text{Mo}_7\text{O}_{24}]^{6-}$  anion opens up a dynamic library by rearrangement into smaller fragments that can then undergo fast combinatorial addition and/or fragmentation to give a diverse range of oligomeric ions of the observed series. The complexity of the library is obvious, and the entire library can be represented by the  $[\text{HMo}_m\text{O}_{3m+1}]^-$  and  $[\text{Mo}_m\text{O}_{3m+1}]^{2-}$  series. It is worth noting that this library already contains the pentagonal building blocks,  $[\text{H}_4\text{Mo}_6\text{O}_{21}(\text{H}_2\text{O})_3] \equiv [(\text{Mo})\text{Mo}_5]$ . The Raman spectrum, on the other hand, shows a typical band around 950  $\text{cm}^{-1}$  ( $\nu_{\text{Mo}=\text{O}}$ ).

Upon addition of the reducing agent,  $\text{N}_2\text{H}_6\text{SO}_4$ , the complexity of the ESI mass spectrum increases with the appearance of new peaks (Figure 2b). Furthermore, at this stage, mixed valent isomolybdate fragments<sup>44</sup> are detected, as well. Molybdenum is found to exist in +V and +VI oxidation states in species such as  $[\text{Mo}_6^{\text{VI}}\text{Mo}^{\text{V}}\text{O}_{21}(\text{CH}_3\text{COO})(\text{H}_2\text{O})_2]^-$ ,  $[\text{Mo}_7^{\text{VI}}\text{Mo}^{\text{V}}\text{O}_{24}(\text{CH}_3\text{COO})(\text{H}_2\text{O})_5]^-$ , etc. This is seen with the change in color of the reaction mixture from colorless to turquoise blue and finally to dark green. Here we observe the condensation of two reduced  $\{\text{Mo}^{\text{V}}\text{O}\}^{3+}$  ions stabilized by an acetate ligand (from ammonium acetate present in the library) to generate a  $\text{HMo}_2\text{V}_2\text{O}_6(\text{CH}_3\text{COO})(\text{H}_2\text{O})_2 \equiv [\text{Mo}_2(\text{acetate})]^-$

linker in the library at  $m/z$  384.75. What happens here is, the starting compound ammonium heptamolybdate is becoming reduced by  $\text{N}_2\text{H}_6\text{SO}_4$ , thus producing  $\text{Mo}^{\text{V}}$  centers in solution (evident from the color change after addition of the reducing agent), which in turn generates  $[\text{Mo}_2(\text{acetate})]$  linkers by condensation.

Moreover, reduction enhances the abundance of the pentagonal  $[(\text{Mo})\text{Mo}_5]$  building blocks, as shown by ESI-MS (Figure 2a,b). Condensation of the building blocks in the library continues, and greater speciation ensues. To determine the real nature of the two main structures involved in the formation of  $[\text{Mo}_{132}]$ , Carr–Parrinello molecular dynamics (MD) simulations<sup>45,46</sup> were performed on the pentagonal unit  $[\text{Mo}_6\text{O}_{21}]^{6-}$  {deprotonated form of  $[\text{H}_4\text{Mo}_6\text{O}_{21}(\text{H}_2\text{O})_3]^{2-}$ } and on dimers with a  $[\text{Mo}_2\text{V}_2\text{O}_8\text{H}_6(\text{CH}_3\text{COO})]^-$  stoichiometry. Combinations of mass spectrometry and Carr–Parrinello molecular dynamics (MD) simulations were shown to be useful for studying molecular oxide fragments in solution.<sup>47,48</sup>

Using a cell box containing initially one starlike hexaprotonated pentagonal unit  $[\text{Mo}_6\text{O}_{15}(\text{OH})_6]$  and 146  $\text{H}_2\text{O}$  molecules ( $a = b = c = 16.90$  Å), a 17 ps simulation was performed (5 ps equilibration with a 12 ps production run). The initial hexaprotonated starlike molybdate releases three protons, yielding  $[\text{Mo}_6\text{O}_{18}(\text{OH})_3]^{3-}$  and three hydronium cations that remain in the solution (Figure 3a). This result indicates that under low-pH conditions the starlike hexamolybdate is protonated with up to three protons. This latter species, which lasts for the whole simulation, is stable at the rather short time scale simulated here. Up to three  $\text{H}_2\text{O}$  molecules interact directly with the different Mo ions of the anion. On average, two  $\text{H}_2\text{O}$  molecules from the solvent are incorporated into the coordination sphere of Mo ions. One of these two aqua ligands is permanently coordinated to the central Mo ion, thus increasing its coordination number to seven. The number of hydroxo ligands attached to the starlike hexamolybdate along the whole simulation is essentially three. These hydroxo ligands are not permanently bonded to the same Mo ions but dynamically change their positions when intramolecular proton transfers take place (see the Supporting Information for a more detailed analysis of MD) (Figure 3a).

To analyze the dimer with a  $[\text{Mo}_2\text{V}_2\text{O}_8\text{H}_6(\text{CH}_3\text{COO})]^-$  stoichiometry, a box ( $a = b = c = 12.58$  Å) containing one  $[\text{Mo}_2\text{V}_2(\mu_2\text{-O})_2(\text{OH})_6(\text{CH}_3\text{COO})]^-$  anion surrounded by 58 water molecules was used. After equilibration for 3 ps, the initial structure of the  $\text{Mo}^{\text{V}}$  dimer is somewhat changed; there is only one oxo bridge between the two  $\text{Mo}^{\text{V}}$  ions, and an intramolecular proton transfer has taken place. Hence, one  $\text{Mo}^{\text{V}}$  ion is six-coordinated by two oxo ligands, two hydroxo ligands, one aqua ligand, and one carboxylato ligand (2O/2OH/1w/

1c), and the other is five-coordinated (2O/2OH/1c). The coordination sphere for each of the two Mo<sup>V</sup> ions is mainly kept during the whole production run (26 ps). The carboxylato ligand is always coordinated to at least one of the two Mo<sup>V</sup> ions, whereas significant changes in the number of oxo, hydroxo, and aqua ligands occur during the simulation, keeping almost constant the total number of ligands at five for one Mo ion and at six for the other (Figure 3b and Figure S1). It is worth mentioning that during the simulation many intramolecular dimer-to-dimer and intermolecular solvent-to-dimer proton transfers are detected. To enhance the sampling, additional production runs were conducted starting from different snapshots of the previous simulation. A 43 ps trajectory has been collected using as an initial structure the [Mo<sup>V</sup><sub>2</sub>O<sub>3</sub>(OH)<sub>4</sub>(H<sub>2</sub>O)(CH<sub>3</sub>COO)]<sup>-</sup> dimer. The coordination environment of the Mo ions along the simulation confirms the dynamical behavior of the dimer that essentially remains with three oxo ligands, four hydroxo ligands, one aqua ligand, and one acetato ligand during the whole simulation. The acetato ligand is also observed now to attach in an asymmetrical manner to each of the Mo<sup>V</sup> ions, with one Mo–O distance that is appreciably longer than the other, confirming its labile character. This, in turn, shows that upon reduction of heptamolybdate a molecular cascade of further condensation opens up, creating larger cluster type species in solution.

**Acidification and Emergence of the [Mo<sub>132</sub>] Raman Spectroscopic Fingerprint.** After reduction, the next synthetic step is acidification. Acidification in the original synthesis is achieved by the addition of acetic acid. Upon acidification, there is a marked decrease in the abundance of [(Mo)Mo<sub>5</sub>] type building blocks in the library. Moreover, larger species like those of [Mo<sub>8</sub>], [Mo<sub>9</sub>], and [Mo<sub>14</sub>] are found. This might be explained as the signature of speciation in the library due to self-condensation and cross-condensation of prime building blocks like [Mo<sub>1</sub>], [Mo<sub>2</sub>], and [(Mo)Mo<sub>5</sub>], respectively. However, the disappearance of the [(Mo)Mo<sub>5</sub>] building block is coupled with an increase in the intensity of the 880 cm<sup>-1</sup> band in the Raman spectrum of the corresponding library. Simulation studies show that band corresponds to the symmetric breathing mode of a large cluster, [Mo<sub>132</sub>]. More precisely, this band corresponds to the symmetric modes of vibrations of μ<sub>2</sub>-O atoms connecting the [(Mo)Mo<sub>5</sub>] units with the linkers.

We have shown the existence of a library in the solution of reduced molybdate. To show how the fragments of that library interact and connect, we computed the Raman spectra of all possible fragments and compared them with that of the experimentally found fragments to show the modality of condensation in forming [Mo<sub>132</sub>] Keplerate cluster (for methodology details, see Experimental Section). It is seen that the pentagonal unit [(Mo)Mo<sub>5</sub>] and the linker [Mo<sub>2</sub>] are both Raman silent. Upon reduction and acidification, the experimental spectra resemble the simulated Raman spectra of condensed pentagonal unit [(Mo)Mo<sub>5</sub>] and linker unit [Mo<sub>2</sub>]. There we observe theoretically a set of new peaks around 650 cm<sup>-1</sup>. The peak with the highest intensity corresponds to the bridging oxygen scissoring and the pentagon nonterminal oxygen bending. Also, we also found the band around 850 cm<sup>-1</sup> due to terminal oxygen stretching. The spectrum is similar to that found experimentally after reduction and acidification of molybdate (Figure 4).

Hence, after reduction and acidification of the starting molybdate solution, it can be said because of Raman spectra

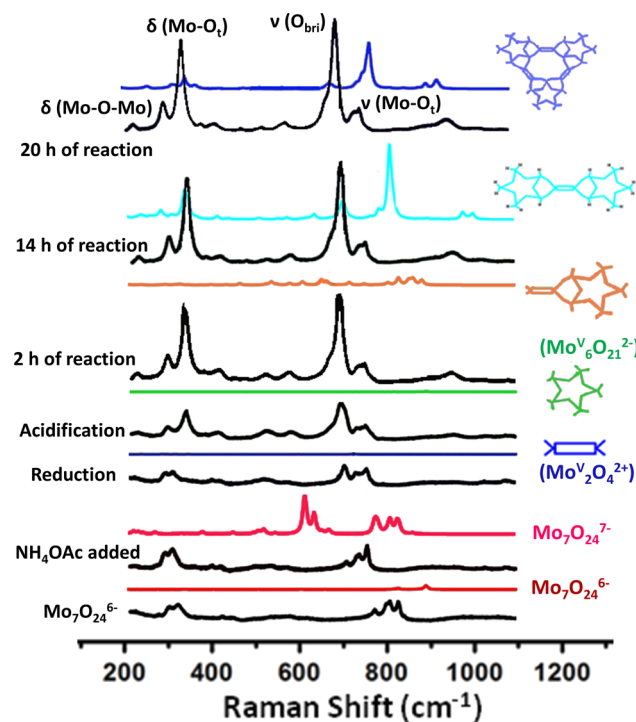


**Figure 4.** Comparison of the evolution of Raman spectra during the formation of [Mo<sub>132</sub>] (black lines) with spectra of several models computed at the DFT level (colored lines). During reaction, the gradual increase in the intensity of four prominent Raman peaks at 314 cm<sup>-1</sup> [ $\delta(\text{Mo}-\text{O}-\text{Mo})$ ], 374 cm<sup>-1</sup> [ $\delta(\text{Mo}-\text{O})$ ], 880 cm<sup>-1</sup> ( $\nu_{\text{O-br}}$ ), and 950 cm<sup>-1</sup> [ $\nu(\text{Mo}-\text{O})$ ] indicates formation of the Mo<sub>132</sub> cluster. See the Supporting Information for details of computed Raman spectra.

that pentagonal unit [(Mo)Mo<sub>5</sub>] and linker unit [Mo<sub>2</sub>] condense. Upon standing, the reaction system evolves further. Raman spectra of time-evolved systems are similar to the simulated spectra of further condensed species. For instance, in the case of two pentagonal units [(Mo)Mo<sub>5</sub>] and linker unit [Mo<sub>2</sub>], the simulated spectra show two peaks due to bridging oxygen wagging modes at 275 cm<sup>-1</sup> (8000 Ang<sup>4</sup>/amu) and 330 cm<sup>-1</sup> (25000 Ang<sup>4</sup>/amu). At 700 cm<sup>-1</sup>, there is a peak due to bridging oxygen symmetric stretching (15000 Ang<sup>4</sup>/amu). The main peak (60000 Ang<sup>4</sup>/amu) is at 813 cm<sup>-1</sup> and corresponds to the pentagon/linker bridging oxygen symmetric stretching. Finally, around 1000 cm<sup>-1</sup>, a set of peaks due to terminal oxygen stretching (6000 Ang<sup>4</sup>/amu) is found, which are similar with the experimentally obtained spectra after samples had been left to stand for 2 h. With further standing, the bands intensify. These spectra in turn resemble the simulated Raman spectra of larger fragments. For instance, the Raman spectra obtained experimentally after reaction for 14 and 20 h resemble closely the simulated spectrum of a [Mo<sub>9</sub>O<sub>9</sub>] pore flanked by three pentagonal [(Mo)Mo<sub>5</sub>] units and three [Mo<sub>2</sub>] linker units. This indicates that in the reaction mixture after 20 h cluster formation is complete and units like that of [Mo<sub>9</sub>O<sub>9</sub>] pores are present and already formed and so is the cluster. This is so because 20 such condensed [Mo<sub>9</sub>O<sub>9</sub>] pores would define a complete [Mo<sub>132</sub>] cluster.

The condensation that leads to the formation of the cluster is mediated by both pH and the degree of reduction. Alone pH causes condensation of mixed valent species to form larger fragments. From pentagonal and linker unit models, we have seen that the condensation energy of the fragments can be very

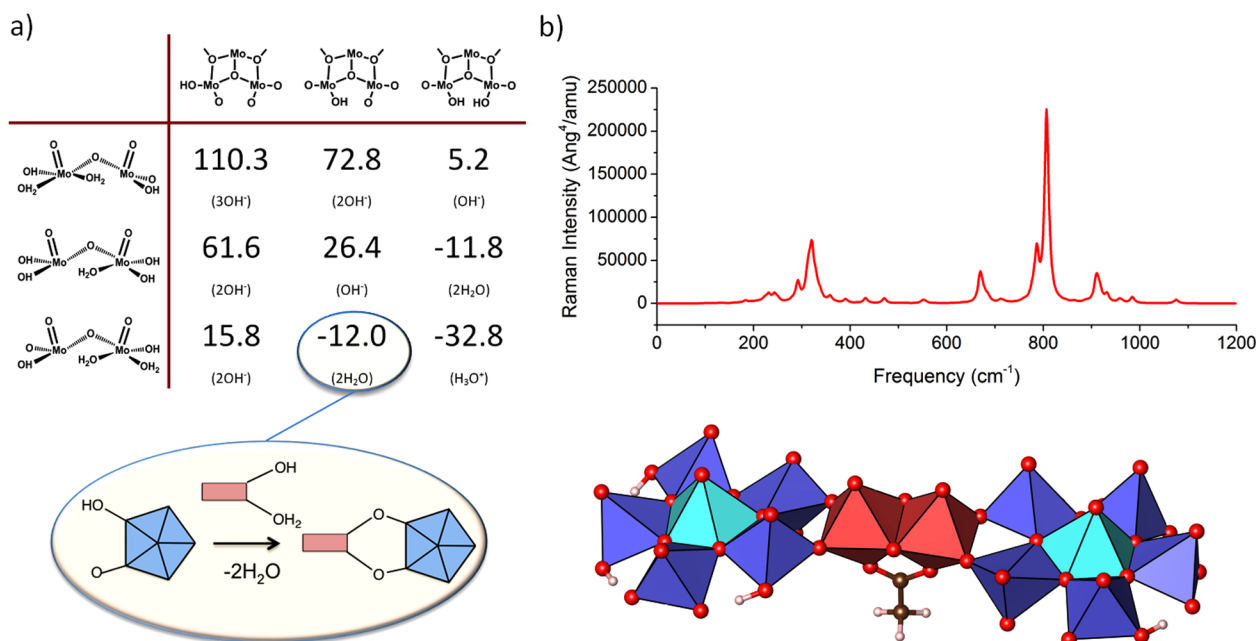


**Figure 5.** (a) Condensation reaction energies (in kilocalories per mole) between dimers (rows)  $[\text{Mo}^{\text{V}}_2\text{O}_3(\text{OH})_4(\text{H}_2\text{O})(\text{CH}_3\text{COO})]^-$  or  $[\text{Mo}^{\text{V}}_2\text{O}_3(\text{OH})_2(\text{H}_2\text{O})_2(\text{CH}_3\text{COO})]^-$  and pentagonal fragments (columns)  $[\text{Mo}^{\text{V}}_2\text{O}_8\text{H}_6(\text{CH}_3\text{COO})]^-$  as a function of the degree of protonation. The inner labels indicate the products obtained upon condensation. Both dimers and pentagonal structures are those suggested by the CP molecular dynamics simulations, and the condensation energies were computed by means of DFT. (b) Theoretical Raman spectrum (top) and schematic representation (bottom) of one of the proposed intermediate systems for  $[\text{Mo}_{132}]$  formation.

depending on the degree of protonation and therefore pH (Figure 5a). Using structures found during the MD trajectories, we have found that the condensation between pentagonal and linker units is exothermic for several linker forms. Hence, formation of a cluster like that of  $[\text{Mo}_{132}]$  is caused by controlled condensation due to reduction and acidification (lowering of pH).

Finally, Raman spectra were computed for a framework that consisted of two pentagonal fragments and a linker-bearing acetate ligand as represented in Figure 5b. The computed Raman spectrum nicely agrees with the experimentally observed spectrum (Figure 4a) and clearly shows that this framework is a key species during the formation of the  $[\text{Mo}_{132}]$  cluster.

The fact that there is an interplay of charge and symmetry in the formation of  $[\text{Mo}_{132}]$  type clusters also emerges. Indeed, it was proposed by the Müller group of Bielefeld that there is a virtual library of building blocks in the solution from which selection takes place. Here we have taken the next steps. We have shown explicitly that a library of building blocks exists. These building blocks are charged and are generated no sooner than the starting precursors are dissolved in water. For instance, pentagonal building block  $[(\text{Mo})\text{Mo}_5]$  exists in this library. Upon reduction of the solution, the population and diversity of building blocks in the library increase. The  $[\text{Mo}_2]$  linker is generated under these conditions by self-condensation of  $[\text{Mo}_1]$  building blocks. Further condensation reactions set in. The combinatorial library experiences an explosion of speciation. Selection sets in. The selection rule operates on charge complementarity. Consequently, pentagonal building blocks like that of  $[(\text{Mo})\text{Mo}_5]$  combine with linkers  $[\text{Mo}_2(\text{acetate})]$  from the library to create a library of larger building blocks like that of  $[\text{Mo}_8]$ . Now it appears that symmetry selection starts operating. More symmetric species with lower surface energies, first  $[(\text{Mo})\text{Mo}_5]$  and then  $[\text{Mo}_2]$

and later  $[\text{Mo}_9\text{O}_9]$  pores with its paraphernalia, lead to the emergence of closed surface entities like that of  $[\text{Mo}_{132}]$ , while the other linear species like those of other isopolymolybdates are depleted. The symmetry selection followed by charge selection indeed operates in a manner of molecular Darwinism and leads to the emergence of a prominent spherical cluster of  $[\text{Mo}_{132}]$  at the expense of other smaller and less symmetric species. This is seen from Raman studies stepwise systematically.

The appearance of various colors during the formation of  $[\text{Mo}_{132}]$  can be shown with the help of electronic absorption spectroscopy (EAS) (Figure 6).

Initially, the solution contains only Mo(VI) fragments for which the solution is colorless. As soon as we add a reducing

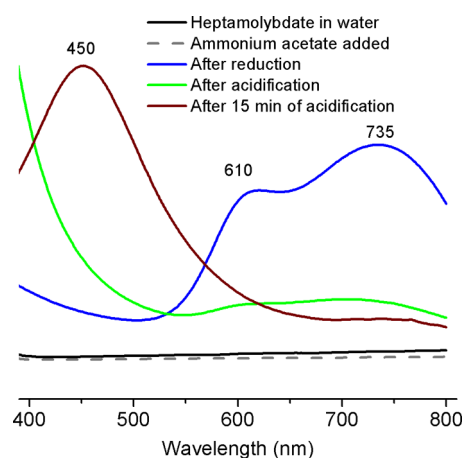


**Figure 6.** Electronic absorption spectroscopy during different steps of the formation of  $[\text{Mo}_{132}]$ . The appearance of various colors is shown during the formation.

agent such as  $\text{N}_2\text{H}_6\text{SO}_4$ , initially a blue color appears because of charge transfer from Mo(V) to Mo(VI) due to the appearance of Mo(V). The solution slowly turns dark green. In EAS at this point, bands at 600 and 735 nm are due to metal–oxo bridge charge transfer and localized oxygen ion vacancies, respectively (Figure 6).<sup>49</sup> After acidification, the solution turns dirty green. At this point, condensation of two Mo(V) units with acetate takes place, which suppresses the bands at 600 and 735 nm as we see in EAS. Soon after acidification, condensation of  $[\text{Mo}_2]$  units with  $[(\text{Mo})\text{Mo}_5]$  starts taking place, turning the solution brown due to the appearance of intervalence charge transfer bands.

## CONCLUSION

In short, we follow the formation pathway of  $[\text{Mo}_{132}]$  Keplerate in water that involves dissolution of heptamolybdate in water. ESI-MS data show that dissolved oxidized molybdate opens a library of building blocks in which pentagonal building block  $[(\text{Mo})\text{Mo}_5]$  is present. Upon reduction, reduced  $[\text{Mo}^{\text{V}}_2\text{O}_2(\text{OH})_6(\text{CH}_3\text{COO})]^-$  type dinuclear linker units with a coordinatively fluxional carboxylate group are formed. Upon acidification, further condensation between the pentagonal building blocks and reduced linkers sets in. We calculate such condensation energies that are favorable only at low or acidic pH. Raman spectroscopic investigations furthermore show stepwise condensation of the units mentioned above to form first condensed  $[(\text{Mo})\text{Mo}_5]$  and  $[\text{Mo}_2]$  units. The reaction system upon standing evolves to form  $[\text{Mo}_9\text{O}_9]$  porelike fragments coronate with three  $[(\text{Mo})\text{Mo}_5]$  and three  $[\text{Mo}_2]$  units, implying formation of a complete cluster.

In conclusion, we have demonstrated the emergence of a closed spherical cluster  $[\text{Mo}_{132}]$ , starting from a reduced and acidified aqueous solution of molybdate. The  $[\text{Mo}_{132}]$  cluster creates confined 3D space by gluing building blocks. Such gluing of building blocks at low pH follows the basic principles of thermodynamics of negative condensation energy. This phenomenon is primarily controlled by charge balance and emergence of more symmetric structures at the expense of less symmetric ones.

## ASSOCIATED CONTENT

### Supporting Information

The Supporting Information is available free of charge on the ACS Publications website at DOI: 10.1021/acs.inorgchem.5b02570.

Detailed description of the Carr–Parrinello molecular dynamics simulations, DFT-based Raman spectral calculations, additional experiments, and a simplified Pourbaix diagram (PDF)

## AUTHOR INFORMATION

### Corresponding Authors

\*E-mail: [pradeep@iit.ac.in](mailto:pradeep@iit.ac.in).

\*E-mail: [cbo@iciq.cat](mailto:cbo@iciq.cat).

\*E-mail: [josepmaria.poblet@urv.cat](mailto:josepmaria.poblet@urv.cat).

\*E-mail: [s.roy@iiserkol.ac.in](mailto:s.roy@iiserkol.ac.in).

### Notes

The authors declare no competing financial interest.

## ACKNOWLEDGMENTS

Atharva Sahasrabudhe and Bibudha Parashar are thanked for the synthesis of the cluster and early experiments during this

project. The authors thank IISER-Kolkata, DST, DST-Fast Track, and BRNS-DAE, India, for financial support. The authors also thank the ICIQ Foundation, the Spanish Ministerio de Economía y Competitividad (MINECO) through Projects CTQ2014-52824-R and CTQ2014-52774-P and the Severo Ochoa Excellence Accreditation 2014-2018 (SEV-2013-0319), and the AGAUR of Generalitat de Catalunya through Projects 2014-SGR-409 and 2014-SGR-199 for financial support. This project was conducted with the support of the COST Action CM1203 “Polyoxometalate Chemistry for Molecular Nanoscience (PoCheMoN)”. S.B. thanks UGC for scholarships, and A.S. thanks CSIR and IIT Madras for scholarships. D.M. gratefully acknowledges the URV-ICIQ fellowship. The authors also thankfully acknowledge the computer resources, technical expertise, and assistance provided by the Barcelona Supercomputing Center-Centro Nacional de Supercomputación.

## REFERENCES

- (1) Pope, M. T.; Müller, A. *Angew. Chem., Int. Ed. Engl.* **1991**, *30*, 34–48.
- (2) Borrás-Almenar, J. J.; Coronado, E.; Müller, A.; Pope, M. *Polyoxometalate Molecular Science*; Springer: Dordrecht, The Netherlands, 2003.
- (3) Carraro, M.; Sandei, L.; Sartorel, A.; Scorrano, G.; Bonchio, M. *Org. Lett.* **2006**, *8*, 3671–3674.
- (4) Rausch, B.; Symes, M. D.; Chisholm, G.; Cronin, L. *Science* **2014**, *345*, 1326–1330.
- (5) Rhule, J. T.; Hill, C. L.; Judd, D. A.; Schinazi, R. F. *Chem. Rev.* **1998**, *98*, 327–358.
- (6) Müller, A.; Sarkar, S.; Shah, S. Q. N.; Bögge, H.; Schmidtman, M.; Sarkar, S.; Kögerler, P.; Hauptfleisch, B.; Trautwein, A. X.; Schünemann, V. *Angew. Chem., Int. Ed.* **1999**, *38*, 3238–3241.
- (7) Müller, A.; Krickemeyer, E.; Bögge, H.; Schmidtman, M.; Peters, F. *Angew. Chem., Int. Ed.* **1998**, *37*, 3359–3363.
- (8) Müller, A. *Nat. Chem.* **2009**, *1*, 13–14.
- (9) Müller, A.; Krickemeyer, E.; Bögge, H.; Schmidtman, M.; Peters, F. *Angew. Chem., Int. Ed.* **1998**, *37*, 3359–3363.
- (10) Roy, S. *CrystEngComm* **2014**, *16*, 4667–4676.
- (11) Roy, S. *Comments Inorg. Chem.* **2011**, *32*, 113–126.
- (12) Biswas, S.; Roy, S. *J. Mater. NanoSci.* **2014**, *1*, 6.
- (13) Verhoeff, A. A.; Kistler, M. L.; Bhatt, A.; Pigga, J.; Groenewold, J.; Klokkenburg, M.; Veen, S.; Roy, S.; Liu, T.; Kegel, W. K. *Phys. Rev. Lett.* **2007**, *99*, 066104.
- (14) Liu, T.; Diemann, E.; Li, H.; Dress, A. W. M.; Müller, A. *Nature* **2003**, *426*, 59–62.
- (15) Judd, B. R. *Proc. R. Soc. London, Ser. A* **1957**, *241*, 122–131.
- (16) Zandi, R.; Reguera, D.; Bruinsma, R. F.; Gelbart, W. M.; Rudnick, J. *Proc. Natl. Acad. Sci. U. S. A.* **2004**, *101*, 15556–15560.
- (17) Rodríguez-Fortea, A.; Alegret, N.; Balch, A. L.; Poblet, J. M. *Nat. Chem.* **2010**, *2*, 955–961.
- (18) Ceulemans, A.; Fowler, P. W. *Nature* **1991**, *353*, 52–54.
- (19) Holton, G. *Am. J. Phys.* **1956**, *24*, 340–351.
- (20) Müller, A. *Science* **2003**, *300*, 749–750.
- (21) Müller, A.; Toma, L.; Bögge, H.; Schmidtman, M.; Kogerler, P. *Chem. Commun.* **2003**, 2000–2001.
- (22) Ziv, A.; Grego, A.; Kopilevich, S.; Zeiri, L.; Miro, P.; Bo, C.; Müller, A.; Weinstock, I. A. *J. Am. Chem. Soc.* **2009**, *131*, 6380–6382.
- (23) Kopilevich, S.; Gil, A.; García-Ratés, M.; Bonet-Avalos, J.; Bo, C.; Müller, A.; Weinstock, I. A. *J. Am. Chem. Soc.* **2012**, *134*, 13082–13088.
- (24) Besson, C.; Schmitz, S.; Capella, K. M.; Kopilevich, S.; Weinstock, I. A.; Kogerler, P. *Dalton Trans.* **2012**, *41*, 9852–9854.
- (25) Garai, S.; Haupt, E. T. K.; Bögge, H.; Merca, A.; Müller, A. *Angew. Chem., Int. Ed.* **2012**, *51*, 10528–10531.
- (26) Grego, A.; Müller, A.; Weinstock, I. A. *Angew. Chem., Int. Ed.* **2013**, *52*, 8358–8362.

- (27) Rezaeifard, A.; Haddad, R.; Jafarpour, M.; Hakimi, M. *J. Am. Chem. Soc.* **2013**, *135*, 10036–10039.
- (28) Garai, S.; Rubčić, M.; Bögge, H.; Gouzerh, P.; Müller, A. *Chem. - Eur. J.* **2015**, *21*, 4321–4325.
- (29) Watfa, N.; Melgar, D.; Haouas, M.; Taulelle, F.; Hijazi, A.; Naoufal, D.; Avalos, J. B.; Floquet, S.; Bo, C.; Cadot, E. *J. Am. Chem. Soc.* **2015**, *137*, 5845–5851.
- (30) Whitesides, G. M.; Ismagilov, R. F. *Science* **1999**, *284*, 89–92.
- (31) Richmond, C. J.; Miras, H. N.; de la Oliva, A. R.; Zang, H.; Sans, V.; Paramonov, L.; Makatsoris, C.; Inglis, R.; Brechin, E. K.; Long, D.-L.; Cronin, L. *Nat. Chem.* **2012**, *4*, 1037–1043.
- (32) Muller, A.; Das, K.; Krickemyer, E.; Kuhlmann, C. Polyoxomolybdate Clusters: Giant wheels and balls. In *Inorganic Syntheses*; John Wiley & Sons, Inc.: New York, 2004; Vol. 34, pp 191–200.
- (33) Long, D.-L.; Streb, C.; Song, Y.-F.; Mitchell, S.; Cronin, L. *J. Am. Chem. Soc.* **2008**, *130*, 1830–1832.
- (34) Wilson, E. F.; Miras, H. N.; Rosnes, M. H.; Cronin, L. *Angew. Chem., Int. Ed.* **2011**, *50*, 3720–3724.
- (35) Nakamura, I.; Miras, H. N.; Fujiwara, A.; Fujibayashi, M.; Song, Y.-F.; Cronin, L.; Tsunashima, R. *J. Am. Chem. Soc.* **2015**, *137*, 6524–6530.
- (36) Poblet, J. M.; Lopez, X.; Bo, C. *Chem. Soc. Rev.* **2003**, *32*, 297–308.
- (37) Lopez, X.; Carbo, J. J.; Bo, C.; Poblet, J. M. *Chem. Soc. Rev.* **2012**, *41*, 7537–7571.
- (38) López, X.; Miró, P.; Carbó, J.; Rodríguez-Forteza, A.; Bo, C.; Poblet, J. *Theor. Chem. Acc.* **2011**, *128*, 393–404.
- (39) Schaffer, C.; Todea, A. M.; Gouzerh, P.; Muller, A. *Chem. Commun.* **2012**, *48*, 350–352.
- (40) Müller, A.; Rehder, D.; Haupt, E. T. K.; Merca, A.; Bögge, H.; Schmidtman, M.; Heinze-Brückner, G. *Angew. Chem., Int. Ed.* **2004**, *43*, 4466–4470.
- (41) Canioni, R.; Marchal-Roch, C.; Leclerc-Laronze, N.; Haouas, M.; Taulelle, F.; Marrot, J.; Paul, S.; Lamonier, C.; Paul, J.-F.; Lorient, S.; Millet, J.-M. M.; Cadot, E. *Chem. Commun.* **2011**, *47*, 6413–6415.
- (42) Wilson, E. F.; Miras, H. N.; Rosnes, M. H.; Cronin, L. *Angew. Chem., Int. Ed.* **2011**, *50*, 3720–3724.
- (43) Vila-Nadal, L.; Wilson, E. F.; Miras, H. N.; Rodríguez-Forteza, A.; Cronin, L.; Poblet, J. M. *Inorg. Chem.* **2011**, *50*, 7811–7819.
- (44) Müller, A.; Roy, S. *Coord. Chem. Rev.* **2003**, *245*, 153–166.
- (45) Car, R.; Parrinello, M. *Phys. Rev. Lett.* **1985**, *55*, 2471.
- (46) Hafner, J. *Nat. Mater.* **2010**, *9*, 690–692.
- (47) Vilà-Nadal, L.; Mitchell, S. G.; Rodríguez-Forteza, A.; Miras, H. N.; Cronin, L.; Poblet, J. M. *Phys. Chem. Chem. Phys.* **2011**, *13*, 20136–20145.
- (48) Vilà-Nadal, L.; Rodríguez-Forteza, A.; Yan, L. K.; Wilson, E. F.; Cronin, L.; Poblet, J. M. *Angew. Chem., Int. Ed.* **2009**, *48*, 5452–5456.
- (49) Conte, M.; Liu, X.; Murphy, D. M.; Taylor, S. H.; Whiston, K.; Hutchings, G. J. *Catal. Lett.* **2016**, *146*, 126–135.